Computers in Earth Science Letters (2026) 67-80

Contents lists available at FoundAE

Computers in Earth Science Letters

Journal homepage: https://ejournal.foundae.com/index.php/cesl/index

Quantifying erosional dissection in the paleovolcanic complex using DEM-based remnant-surface reconstruction and kriging

Rizqi Prastowo[a,*], Ignatius Adi Prabowo[b]

[a] Department of Mining Engineering, Faculty of Engineering and Planning, Institut Teknologi Nasional Yogyakarta, Sleman, Yogyakarta 55281, Indonesia

[b] Faculty of Built Environment and Surveying, Universiti Teknologi Malaysia, Johor Bahru, Johor 81310, Malaysia

ARTICLE INFO

Keywords:
DEMNAS;
Erosional dissection;
Geostatistical reconstruction;
Kulon Progo paleovolcanoes;
Ordinary kriging;
Remnant surfaces.

ABSTRACT

Quantifying erosional dissection in deeply eroded volcanic landscapes remains challenging because preserved topographic surfaces are spatially fragmented and the original volcanic morphology is poorly constrained. This study develops and evaluates a digital elevation model (DEM)-based approach for reconstructing remnant-surface envelopes and estimating erosion-related topographic volume loss in the Kulon Progo paleovolcanic complex, Indonesia. The Indonesian National Digital Elevation Model (DEMNAS), resampled to 16 m resolution, was analyzed across a 590.8 km² volcanic massif. Potential remnant surfaces were identified using five terrain criteria: relative topographic position, topographic position index, distance from drainage channels, vector ruggedness measure, and surface curvature. Selected surface elevations were aggregated into control points and interpolated using ordinary kriging with a power variogram. Reconstruction performance was evaluated through spatial block cross-validation and comparison with inverse distance weighting (IDW), while alternative surface-selection thresholds were used to assess volume sensitivity. The principal selection criteria identified 51.6 km² of potential remnant surfaces, representing 8.7% of the massif. Kriging achieved a cross-validation root mean square error of 35.6 m (R^2 = 0.95), representing a 24.6% reduction in RMSE compared with IDW (47.2 m). The reconstructed envelope yielded an estimated eroded volume of 25.7 km³, equivalent to a mean erosion thickness of approximately 43 m and a model-derived denudation ratio of 20.2%. Alternative remnant-selection thresholds produced volume estimates ranging from 14.4 to 43.7 km³, whereas a summit-envelope reconstruction yielded 100.3 km³. Andesitic intrusive units exhibited greater median reconstructed erosion thickness (54 m) than the Kebobutak Formation (25 m), although this contrast cannot be attributed solely to differences in lithological resistance. These findings demonstrate the potential of DEM-based kriging reconstruction for quantifying landscape dissection while emphasizing the sensitivity of estimated erosion volumes to surface-selection criteria and reconstruction assumptions.

1. Introduction

Volcanic landscapes undergo substantial morphological transformation following the cessation of volcanic activity, as prolonged weathering, fluvial incision, mass wasting, and tectonic deformation progressively modify their original constructional surfaces. Over geological timescales, these processes may substantially reduce volcanic edifices, expose their internal structures, and produce complex landscapes in which the original volcanic morphology is no longer readily recognizable. Quantifying the magnitude of erosional modification is therefore essential for understanding the long-term geomorphological evolution of volcanic terrains. Digital elevation models (DEMs) have increasingly facilitated quantitative investigations of volcanic morphology by providing spatially continuous information on elevation, terrain geometry, and landscape dissection [1, 2]. Nevertheless, reconstructing the volume of material removed from deeply eroded volcanic systems remains challenging because the former reference surface is generally incompletely preserved.

Previous studies have demonstrated that DEM-based approaches can provide valuable constraints on volcanic morphology and long-term erosion. Grosse et al. [1] established a systematic framework for characterizing volcanic edifices through quantitative morphometric analysis, while Karátson et al. [2] investigated erosion patterns and rates in volcanic landscapes using DEM-derived topographic information.

* Corresponding author.
E-mail address: rizqi@itny.ac.id (R. Prastowo).

https://doi.org/10.58524/cesl.v1i2.197
Received 20 June 2026; Received in revised form 15 July 2026; Accepted 28 August 2026
Available online 30 September 2026
3163-3579/Published by FoundAE (Foundation of Advanced Education).

Lahitte et al. [3] further demonstrated the application of DEM-based reconstruction to volcanic edifice evolution and estimates of volcanic construction. Collectively, these studies highlight the potential of terrain analysis for investigating volcanic landscape transformation. However, the reliability of reconstructed erosion volumes depends fundamentally on the representation of the reference surface against which present-day elevation is compared. This problem becomes particularly important in ancient volcanic complexes where constructional surfaces have undergone substantial erosion, deformation, and modification by subsequent geological processes [3–5].

One approach to evaluating erosional modification involves reconstructing an upper topographic envelope from preserved landscape elements. Broad ridge crests, relatively smooth interfluves, and elevated terrain surfaces may retain partial information about the topography that existed before the incision of the present drainage network. By interpolating elevations across these preserved elements, a continuous reference surface can be constructed and compared with the existing DEM to estimate the volume of topographic material removed beneath the reconstructed envelope. Related approaches have been applied to investigate relief development and landscape modification in mountainous environments [4,5]. Nevertheless, the interpretation of such envelopes requires caution. Preserved interfluves do not necessarily represent an unmodified original surface, and their elevations may reflect differential erosion, lithological variability, structural deformation, and subsequent landscape adjustment. Consequently, an interpolated envelope is more appropriately interpreted as a model-dependent representation of a former or less-dissected terrain configuration rather than a direct reconstruction of the original volcanic edifice [6, 7].

The identification of potentially preserved surfaces represents a critical step in this reconstruction process. In deeply dissected terrain, remnants of relatively continuous upper surfaces may be distinguished from incised valleys and irregular hillslopes using combinations of geomorphometric attributes. Relative topographic position, the topographic position index (TPI), surface ruggedness, curvature, and proximity to drainage channels provide complementary descriptions of local terrain configuration. TPI has been widely applied to differentiate elevated landforms, valley positions, and intermediate terrain settings across heterogeneous landscapes [6]. Similarly, the vector ruggedness measure (VRM) provides a quantitative representation of terrain surface complexity by evaluating the dispersion of surface-normal vectors [7]. When integrated with relative elevation and drainage-network information, these attributes can support the systematic identification of candidate remnant surfaces. However, the selection of attribute thresholds remains a source of methodological uncertainty because alternative criteria may identify different proportions and spatial distributions of potentially preserved terrain [8–10].

After identifying candidate remnant surfaces, a major challenge is reconstructing elevations across intervening areas where the reference surface is no longer preserved. Geostatistical interpolation provides a framework for estimating spatially distributed elevations from geographically dispersed observations. Kriging, originating from the principles of regionalized-variable theory developed by Matheron [8], incorporates spatial dependence through a semivariogram and produces predictions based on weighted combinations of surrounding observations. Oliver and Webster [9] described the application of kriging as a spatial interpolation technique for geographical information systems. Compared with deterministic approaches such as inverse distance weighting (IDW), kriging additionally provides a model-based estimate of prediction uncertainty. Variogram modeling is therefore an important component of the reconstruction procedure, as the assumed spatial covariance structure influences predicted elevations and their associated uncertainty. Weighted least-squares approaches have been developed to fit theoretical models to experimental semivariograms [10], providing a basis for parameter estimation in geostatistical applications [3, 11].

Despite these advantages, applying kriging to volcanic terrain reconstruction introduces several important considerations. Volcanic landscapes frequently exhibit strong regional elevation gradients, pronounced topographic anisotropy, and spatially heterogeneous terrain properties. These characteristics may complicate the assumptions underlying ordinary kriging, particularly where the spatial variation of the reference surface contains a substantial deterministic trend. In addition, remnant-surface observations are rarely distributed uniformly across a landscape. They may be concentrated along relatively broad ridges and elevated surfaces, leaving deeply incised sectors with limited direct elevation constraints. Consequently, interpolation performance measured at observed remnant surfaces may differ from the reliability of reconstruction within valleys where the former surface is no longer preserved. Spatially structured validation is therefore important because conventional random cross-validation may overestimate predictive performance when geographically adjacent observations contain strongly correlated information [11]. Even when spatial cross-validation demonstrates satisfactory predictive accuracy, the geological interpretation of the reconstructed envelope remains dependent on the validity of the selected control surfaces [12, 13].

The Kulon Progo Mountains, located west of Yogyakarta in southern Java, Indonesia, provide a suitable geological setting for investigating these methodological challenges. The region comprises a strongly eroded Oligocene–Miocene volcanic complex that has undergone prolonged tectonic and geomorphological modification. Van Bemmelen [12] described the broader geological evolution of Java, including the tectonic and volcanic development of the Kulon Progo region. Subsequent geological investigations have emphasized the structural complexity and volcanic characteristics of this area [13]. More recent volcanostratigraphic interpretation recognizes the Gajah, Ijo, and Menoreh volcanic assemblages within the Kulon Progo complex [14]. The prolonged modification of these volcanic landforms has produced deeply incised drainage networks, dissected volcanic ridges, relatively preserved elevated surfaces, and exposures of intrusive and volcanic rock units. These characteristics make the region particularly relevant for evaluating whether a morphometrically defined remnant-surface envelope can provide useful quantitative information on landscape dissection [6, 14, 15].

The geological framework further complicates the interpretation of erosional modification. According to the regional geological map of the Yogyakarta Quadrangle [15], the Kulon Progo complex includes the Kebobutak Formation, andesitic and dacitic intrusive bodies, and the Jonggrangan Formation. These units differ in geological origin, distribution, and geomorphological setting. The present topography may therefore reflect interactions among volcanic construction, tectonic uplift, erosion, lithological heterogeneity, and weathering rather than a uniform history of material removal. Differences in reconstructed erosion thickness among geological units could potentially provide information about landscape modification. However, such differences cannot be attributed directly to contrasting rock resistance without considering initial topographic position, spatial variations in drainage dissection, geological boundary uncertainty, and the distribution of remnant-surface control points.

The Indonesian National Digital Elevation Model (DEMNAS) provides an opportunity to investigate these questions at relatively high spatial resolution. DEMNAS integrates elevation information from multiple remote-sensing sources and supports

quantitative terrain analysis across the Indonesian archipelago. Nevertheless, its representation of the actual ground surface requires careful consideration, particularly in densely vegetated environments where elevation values may partly reflect aboveground features. Julzarika and Harintaka [16] examined the distinction between digital surface and terrain characteristics in DEMNAS, emphasizing issues relevant to the interpretation of derived geomorphometric attributes. Furthermore, the spatial resolution of the DEM, terrain smoothing, drainage extraction, and neighborhood sizes used for attribute calculation may influence the selection of remnant surfaces and ultimately the reconstructed erosion volume. These considerations highlight the need to evaluate the robustness of DEM-based reconstructions rather than relying exclusively on a single interpolated surface.

Although DEM-based volcanic morphology and landscape reconstruction have been investigated in previous studies, the combined effects of morphometric remnant selection, spatial interpolation, and reconstruction uncertainty remain important challenges in deeply eroded tropical paleovolcanic landscapes. In particular, three questions require investigation: (1) whether candidate remnant surfaces can be systematically identified from DEM-derived terrain characteristics; (2) how reliably a continuous terrain envelope can be estimated from spatially fragmented control surfaces; and (3) how sensitive the resulting erosion-volume estimates are to remnant-selection criteria and reconstruction assumptions. Addressing these questions is necessary to distinguish measurable terrain dissection from more speculative interpretations of total volcanic edifice degradation.

This study aims to quantify model-derived erosional dissection within the Kulon Progo paleovolcanic complex using DEMNAS-based morphometric analysis and kriging reconstruction of remnant-surface envelopes. Specifically, the objectives are to (1) identify candidate remnant surfaces using five complementary terrain criteria, including relative position, TPI, drainage distance, surface ruggedness, and curvature; (2) reconstruct a spatially continuous remnant-surface envelope using ordinary kriging and evaluate interpolation performance through spatial block cross-validation and comparison with IDW; (3) estimate reconstructed erosion thickness, removed terrain volume, and a model-derived denudation ratio; and (4) evaluate the sensitivity of these estimates to alternative surface-selection thresholds and examine their spatial variation across mapped geological units. By explicitly distinguishing interpolation performance, reconstruction assumptions, and geological interpretation, this study seeks to establish a reproducible framework for evaluating erosional dissection in deeply modified volcanic landscapes without assuming that the reconstructed envelope represents the original volcanic constructional surface.

2. Method

2.1. Study area and geological framework

The study was conducted in the Kulon Progo paleovolcanic complex, located west of Yogyakarta in the southern part of Java, Indonesia. The study region encompasses a deeply eroded volcanic massif characterized by dissected ridges, incised valleys, relatively preserved upland surfaces, and intrusive rock exposures. The regional geological framework reflects the prolonged interaction of Oligocene–Miocene volcanism, tectonic deformation, uplift, and subsequent landscape modification [12–15]. The analysis was restricted to the volcanic massif represented within DEMNAS tiles 1408-21 and 1408-23, covering approximately 110.00–110.25° E and 7.50–8.00° S. The selected DEM coverage encompasses most of the Kulon Progo volcanic dome, although a narrow sector along its western margin lies outside the analyzed tiles. The spatial extent and geological configuration of the study area are illustrated in Fig. 1.

The volcanic massif boundary was delineated using the digital geological dataset distributed by the Geological Research and Development Centre, Geological Agency of Indonesia [17], with lithological classifications corresponding to the Geological Map of the Yogyakarta Quadrangle [15]. The mapped volcanic massif covers approximately 590.8 km² and comprises four principal geological units. The Kebobutak Formation (Tomk) occupies the largest proportion of the massif (69.3%), followed by andesitic intrusions (a1; 25.3%), the Jonggrangan Formation (Tmj; 4.3%), and dacitic intrusions (da; 1.1%).

The selected geological units exhibit different spatial distributions and topographic expressions. The Kebobutak Formation forms much of the volcanic terrain, while andesitic intrusive bodies occur within several dissected mountainous sectors. The Jonggrangan Formation is associated with relatively elevated parts of the landscape, whereas dacitic intrusions occupy comparatively limited areas. These geological units were used to evaluate the spatial distribution of reconstructed erosion thickness. Geological formation labels were not used to determine remnant-surface thresholds or to train the interpolation model.

The study focused on reconstructing an upper terrain envelope based on potentially preserved surfaces. This envelope was intended to represent a model-dependent reference for quantifying present-day topographic dissection, rather than the original constructional surface of the Oligocene–Miocene volcanic edifices.

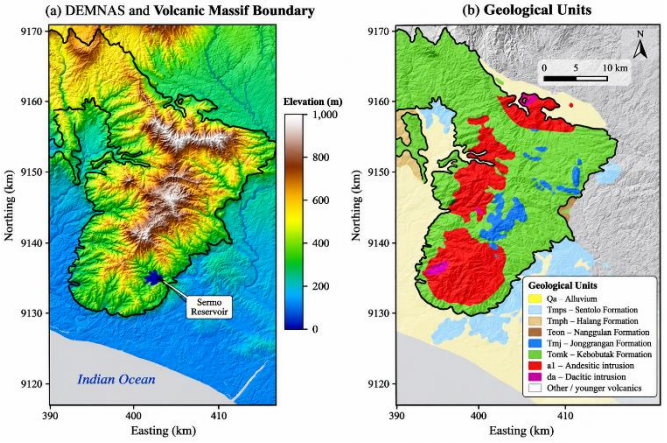


Fig. 1. Location and geological setting of the Kulon Progo paleovolcanic complex, Indonesia: (a) DEMNAS-derived elevation and the volcanic massif boundary (black outline), and (b) geological units obtained from the regional digital geological map [17]. Coordinates are presented in WGS 84/UTM Zone 49S.

2.2. DEMNAS data and terrain preprocessing

Topographic information was obtained from the Indonesian National Digital Elevation Model (DEMNAS), provided by the Geospatial Information Agency of Indonesia (Badan Informasi Geospasial, BIG). The source DEMNAS dataset has a nominal horizontal resolution of approximately 0.27 arcseconds, corresponding to approximately 8 m in the study region, and uses the Earth Gravitational Model 2008 (EGM2008) as its vertical reference. DEMNAS incorporates elevation information from multiple remote-sensing datasets, including IFSAR, TerraSAR-X, and ALOS PALSAR, as described in previous assessments of Indonesian elevation data [16,18].

Although DEMNAS provides relatively detailed topographic coverage, its elevation values may be affected by vegetation and other aboveground features, particularly in densely forested environments [16]. Such effects are relevant to this study because surface ruggedness and curvature were used to identify candidate remnant surfaces. The two DEMNAS tiles were mosaicked and

aggregated to a uniform 16 m grid in the WGS 84/UTM Zone 49S coordinate system. The resulting raster provided the common elevation framework for morphometric analysis, drainage-network extraction, identification of remnant surfaces, and erosion-volume integration.

The landward volcanic massif was delineated using the regional geological polygons. Marine areas and the Sermo Reservoir were excluded from the analysis. The excluded reservoir covered approximately 0.81 km². The digital elevation data were subsequently used to calculate terrain attributes describing elevation position, surface texture, and drainage proximity. Drainage-network extraction was performed using a depression-filled DEM. Flow direction was determined using the deterministic eight-neighbor (D8) routing algorithm of O'Callaghan and Mark [19]. Raster cells with an upstream contributing area of at least 0.05 km² were classified as drainage-channel cells.

The resulting channel network provided a spatial reference for calculating the distance between individual terrain cells and the nearest extracted channel. All geospatial processing, terrain calculations, interpolation, and volumetric analysis were conducted using Python. The analytical workflow consisted of DEM preparation, extraction of terrain attributes, remnant-surface selection, elevation-control aggregation, semivariogram modeling, ordinary kriging, spatial cross-validation, erosion-volume estimation, and sensitivity analysis (Fig. 2).

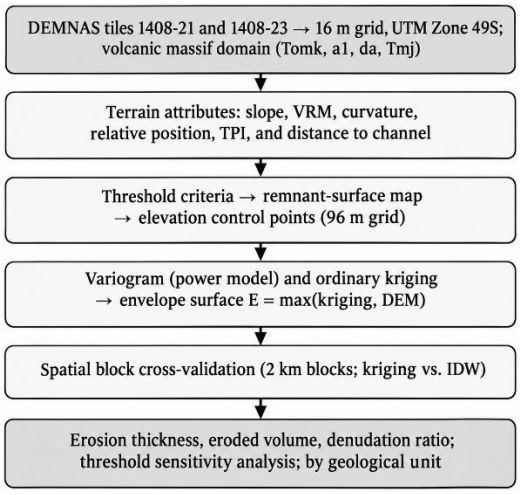


Fig. 2. Workflow of DEMNAS-based remnant-surface identification and kriging reconstruction. The procedure includes DEM preparation, extraction of five terrain attributes, remnant-surface selection under alternative threshold scenarios, aggregation into elevation control points, semivariogram fitting, ordinary kriging, spatial block cross-validation, reconstruction of a nonnegative erosion-thickness surface, and estimation of erosion volume and geological-unit-specific characteristics.

2.3. *Morphometric identification of candidate remnant surfaces*

Candidate remnant surfaces were identified from DEM-derived terrain characteristics. The underlying assumption was that relatively preserved interfluves and upper terrain surfaces would exhibit smoother morphology, limited curvature, relatively elevated positions within their local surroundings, and greater separation from incised drainage channels.

Five terrain criteria were selected to represent these characteristics: relative position (RP), topographic position index (TPI), distance to the nearest drainage channel, vector ruggedness measure (VRM), and surface curvature. These criteria were used as a rule-based screening procedure. Their combination was intended to identify candidate remnant surfaces systematically rather than to establish their geological age or confirm that they belonged to a single original topographic surface [4, 16].

2.3.1. *Relative position and topographic position index*

Relative position (RP) was calculated to describe the normalized elevation of each cell within its surrounding terrain. The index was defined as:

$$RP_{(x)} = (z_{(x)} - z_{min(x)}) / (z_{max(x)} - z_{min(x)}) \quad \ldots (1)$$

where $z_{(x)}$ is the elevation at location (x), (z_{min}) and (z_{max}) represent the minimum and maximum elevations within the corresponding neighborhood. Higher RP values indicate locations closer to the upper portion of the local elevation range, whereas lower values indicate relatively depressed terrain positions. The topographic position index (TPI) was calculated as the difference between the elevation of a cell and the mean elevation within its surrounding neighborhood [6].

$$TPI_{(x)} = z_{(x)} - \bar{z}_{N(x)} \quad \ldots (2)$$

where $\bar{z}_{N(x)}$ represents the mean elevation within neighborhood $(N_{(x)})$. Positive TPI values indicate locations higher than their surrounding terrain, whereas negative values indicate relatively lower topographic positions. Both RP and TPI were calculated using a 2 km neighborhood, providing complementary information about the relative position of terrain cells within the broader landscape. The main remnant-selection rule required RP ≥ 0.5 and TPI ≥ 0 m. These conditions favored upper topographic positions while reducing the inclusion of deeply incised valley floors.

2.3.2. *Surface ruggedness and curvature*

Surface ruggedness was quantified using the vector ruggedness measure proposed by Sappington et al. [7]. VRM evaluates the variability of surface orientation within a neighborhood using three-dimensional unit normal vectors:

$$VRM = 1 - |\Sigma n_i| / n \quad \ldots (3)$$

where $|\Sigma n_i|$ is the unit surface-normal vector of cell (i), and (n) is the total number of cells within the analysis window.

VRM was calculated using a 5 × 5 cell neighborhood on the processed elevation grid. Lower VRM values indicate relatively uniform surface orientations, whereas higher values reflect greater variability in terrain surface orientation. Surface curvature was calculated using the polynomial terrain-fitting method of Zevenbergen and Thorne [20]. Profile and plan curvature were combined into a curvature-magnitude descriptor used to characterize deviations from relatively smooth terrain surfaces.

Slope gradients were calculated using the Horn finite-difference operator [21] as part of the terrain-derivative workflow. The remnant-surface screening favored cells with relatively low ruggedness and curvature values. These properties were intended to reduce the selection of sharply dissected terrain, although low ruggedness and curvature alone do not demonstrate preservation of an older geomorphic surface.

2.3.3. *Distance from drainage channels*

The distance to the nearest extracted drainage channel was used to reduce the likelihood of selecting terrain strongly affected by contemporary channel incision. The channel network was obtained from the depression-filled DEM using D8 flow routing [19], with channel initiation defined by an upstream contributing area of at least 0.05 km². For each terrain cell, the distance to the

nearest channel was calculated spatially. Cells located farther from extracted channels were considered more likely to belong to relatively preserved interfluves. The main selection rule required a minimum channel distance of 100 m. This criterion was intended to reduce the influence of incised valley floors and adjacent valley slopes. However, its effectiveness depends on the drainage extraction procedure and the selected channel-initiation threshold.

2.3.4. Threshold-based remnant-surface selection

A cell was classified as a candidate remnant surface only when it satisfied all five terrain criteria simultaneously. The primary threshold scenario required RP ≥ 0.5, TPI ≥ 0 m, distance to the nearest channel ≥ 100 m, VRM ≤ 0.0058, and combined curvature magnitude ≤ 0.43 in the units reported by the original analysis. The VRM and curvature thresholds were selected using the median values calculated across the volcanic massif. This provided a relative screening criterion based on the distribution of terrain attributes within the study region.

To evaluate sensitivity to threshold selection, two alternative scenarios were defined. The strict scenario applied a higher relative-position threshold (RP ≥ 0.6), a larger minimum channel distance (150 m), and lower limits for VRM and curvature corresponding to their 40th-percentile values. The relaxed scenario reduced the relative-position threshold to RP ≥ 0.4, allowed cells at least 50 m from extracted channels, and increased the VRM and curvature limits to their 60th-percentile values. The TPI threshold remained unchanged across all scenarios at TPI ≥ 0 m. The complete threshold criteria are summarized in Table 1.

Table 1
Threshold criteria for identifying candidate remnant surfaces

Terrain criterion	Primary scenario	Strict scenario	Relaxed scenario
Relative position (RP), 2 km neighborhood	≥ 0.5	≥ 0.6	≥ 0.4
Topographic position index (TPI), 2 km neighborhood	≥ 0 m	≥ 0 m	≥ 0 m
Distance to nearest drainage channel (m)	≥ 100	≥ 150	≥ 50
Vector ruggedness measure (VRM)	≤ 0.0058 (median)	≤ 0.0046 (P40)	≤ 0.0073 (P60)
Combined surface curvature (1/100 m)	≤ 0.43 (median)	≤ 0.38 (P40)	≤ 0.48 (P60)

Note: *RP = relative position; TPI = topographic position index; VRM = vector ruggedness measure. P40, P50 (median), and P60 represent the 40th, 50th, and 60th percentiles, respectively, of the corresponding terrain attributes within the volcanic massif. Candidate remnant surfaces were identified only when all five criteria were satisfied simultaneously. Remnant-surface patches smaller than 0.01 km² were excluded before aggregation into elevation control points.*

Following threshold screening, remnant-surface patches smaller than 0.01 km² were removed. This step was intended to eliminate isolated small patches and retain more spatially continuous candidate surfaces for subsequent elevation-envelope reconstruction. The remnant-surface masks were generated independently for the primary, strict, and relaxed scenarios. Their spatial distributions and corresponding reconstruction results were subsequently compared to evaluate the sensitivity of the estimated erosion volume to surface-selection criteria.

2.4. Spatial aggregation and elevation control-point generation

The selected remnant-surface cells were aggregated into spatially distributed elevation control points for geostatistical interpolation. Aggregation was performed using a regular 96 m block structure. Each block containing at least four selected remnant-surface cells contributed one elevation control point. The horizontal position and elevation of each control point were calculated from the mean coordinates and mean elevations of the qualifying remnant-surface cells within the corresponding block.

This aggregation procedure reduced the number of closely spaced elevation observations while retaining a spatial representation of the selected candidate surfaces. Control-point aggregation was applied separately to the three remnant-selection scenarios. As a result, the number and spatial distribution of control points varied according to the selected threshold criteria.

For the primary scenario, the procedure produced 10,288 elevation control points. The strict and relaxed scenarios produced 3,595 and 20,234 points, respectively. These differences were retained in the subsequent interpolation and sensitivity analyses. The aggregation scale was fixed at 96 m in the original analysis. Its influence on the final reconstruction was not independently evaluated through alternative block sizes.

Furthermore, because the control points were derived exclusively from terrain satisfying the remnant-selection criteria, their distribution was not spatially uniform. The control network was expected to be denser in relatively preserved uplands and less extensive in strongly dissected sectors. The resulting interpolated elevations should therefore be understood as predictions based on a spatially selective control network rather than on direct measurements of former terrain elevations throughout the entire volcanic massif [17, 18].

2.5. Semivariogram modeling and ordinary kriging reconstruction

The spatial dependence of control-point elevation was evaluated using an experimental semivariogram [19–21]. The semivariance at separation distance (h) was calculated as:

$$\gamma(h) = [1 / 2N(h)] \Sigma [z(x_i) - z(x_i + h)]^2 \quad \ldots (4)$$

where $N(h)$ is the number of observation pairs separated by distance (h), and $z(x_i)$ and $z(x_i + h)$ represent their respective elevations. The experimental semivariogram was evaluated over separation distances extending from approximately 200 m to 6 km. The semivariance increased continuously with separation distance over the investigated range and did not exhibit a clearly defined sill. Accordingly, a power variogram model was adopted to describe the observed spatial dependence [14, 22]. The selected theoretical model was:

$$\gamma(h) = c_0 + bh^{\alpha}, \quad 0 < \alpha < 2 \quad \ldots (5)$$

where c_0 is the nugget parameter, (b) is a scale coefficient, and α controls the rate at which semivariance increases with distance.

The power variogram parameters were fitted using weighted least squares, following the geostatistical approach described by Cressie [10]. The power model was used because it reproduced the increasing experimental semivariance observed within the selected distance range. However, its use does not independently establish that the regional elevation trend satisfies the assumptions of ordinary kriging. The reconstructed surface was therefore interpreted as a conditional spatial prediction based on the selected control points and variogram specification.

2.5.1. Ordinary kriging interpolation

Elevation-envelope reconstruction was performed using ordinary kriging, a geostatistical interpolation method that estimates unknown values from spatially dependent observations [8, 9]. For an unsampled location (x_o), the predicted envelope elevation was calculated as:

$$\hat{Z}(x_o) = \Sigma \lambda_i z(x_i), \quad \Sigma \lambda_i = 1 \quad \ldots (6)$$

where $\hat{Z}(x_o)$ is the predicted elevation, $z(x_i)$ represents the observed

elevation at control point (i), (λ_i) is the kriging weight assigned to that observation, and (n) is the number of neighboring observations. For each prediction location, the 24 nearest elevation control points were used to construct the local kriging system.

The interpolation weights were determined from the fitted semivariogram and the ordinary kriging constraints. The calculation also provided a kriging prediction standard deviation, denoted by σK. The kriging envelope was first predicted on a 100 m grid and subsequently resampled to match the 16 m DEM analysis grid. The use of a 100 m prediction grid provided a computationally manageable interpolation framework, although resampling to 16 m did not generate new independent spatial information beyond the original kriging predictions. The same general reconstruction workflow was applied to the primary, strict, and relaxed remnant-surface scenarios.

2.5.2. Nonnegative erosion-thickness constraint

An unconstrained interpolated envelope may lie below the observed terrain in some locations because the predicted surface is derived from a spatially limited set of control points. For the purpose of calculating nonnegative erosion thickness, the final reference envelope was defined as:

$$E(x) = max\,[\hat{Z}(x), z(x)] \quad \ldots (7)$$

where $E(x)$ is the corrected reference envelope, $\hat{Z}(x)$ is the ordinary kriging prediction, and $z(x)$ represents the present-day DEM elevation.

This operation imposed the condition that the reference envelope could not lie below the observed terrain. The correction was introduced as a numerical constraint for calculating erosion thickness and should not be interpreted as independent geological evidence of the former terrain surface. The resulting envelope represents a spatially modeled upper reference surface conditioned on the selected remnant observations, the fitted variogram, and the imposed nonnegative thickness constraint.

2.6. Spatial block cross-validation and interpolation performance

The predictive performance of ordinary kriging was evaluated using five-fold spatial block cross-validation. Spatial blocks with dimensions of 2 × 2 km were used to partition the available elevation control points into geographically structured validation subsets. This approach was selected to reduce the effects of spatial dependence between training and validation observations, which can cause conventional random cross-validation to produce overly optimistic performance estimates for spatial prediction problems [11]. For each cross-validation iteration, a subset of control-point observations was withheld, and the interpolation model was evaluated by comparing predicted elevations with observed elevations at the withheld locations [14, 22]. The overall prediction error was summarized using root mean square error (RMSE):

$$Root\ Mean\ Squared\ Error\ (RMSE) = \sqrt{\frac{1}{N}\sum_{i=1}^{N}(z_i - \hat{z}_i)^2} \quad \ldots (7)$$

where z_i and $\hat{Z}_i$ are the observed and predicted elevations at withheld control points, respectively, and (N) is the number of evaluated observations. Mean prediction error was calculated as:

$$ME = \frac{1}{N}\sum_{i=1}^{N}\hat{z}_i - z_i \quad \ldots (8)$$

to assess systematic prediction bias. The coefficient of determination R^2 was also calculated to summarize agreement between observed and predicted elevations:

$$\text{Coefficient of determination } (R^2) = 1 - \frac{\frac{1}{N}\sum_{i=1}^{N}(z_i - \hat{z}_i)^2}{\frac{1}{N}\sum_{i=1}^{N}(z_i - \bar{z})^2} \quad \ldots (9)$$

where $\bar{z}$ is the mean elevation of the evaluated observations. Ordinary kriging was compared with inverse distance weighting (IDW), using an inverse-distance exponent of 2. The IDW approach follows the deterministic spatial interpolation principle introduced by Shepard [22]. The reported performance comparison was based on the same remnant-control dataset and spatial validation framework.

The agreement between observed elevations and kriging prediction intervals was evaluated by calculating the proportion of withheld observations falling within $\hat{Z}(xi) \pm 1.96\ \sigma K\ (xi)$. This provided an empirical assessment of the nominal pointwise prediction interval coverage at withheld remnant-control locations. However, cross-validation at remnant-surface points evaluates interpolation accuracy for the selected observations. It does not directly establish the accuracy of reconstructed elevations within deeply incised valleys where the former reference surface is no longer preserved.

Similarly, prediction intervals derived from the kriging model characterize uncertainty conditional on the adopted spatial covariance model and observation network. They do not encompass all geological and methodological uncertainties associated with reconstructing a former landscape surface.cost [6, 14, 15].

2.7. Reconstruction of erosion thickness, volume, and denudation ratio

The corrected remnant-surface envelope was compared with present-day topography to estimate the thickness of terrain located below the reconstructed reference surface. Erosion thickness was calculated for each valid analysis cell as:

$$T(x) = E(x) - z(x) \quad \ldots (10)$$

where $T(x)$ is the estimated erosion thickness, $E(x)$ is the corrected envelope elevation, and $z(x)$ is the present-day elevation. By construction, T(x) ≥ 0 throughout the analyzed region. The total reconstructed erosion volume was calculated by spatially integrating erosion thickness:

$$V = \sum_{i=1}^{N} T_i\ A_i \quad \ldots (11)$$

where (V) is the reconstructed erosion volume, (Ti) is the erosion thickness of cell (i), and (Ai) is the corresponding cell area. For a complete 16 m analysis cell, the nominal area was A= 16 x 16 = 256 m². The resulting volume was expressed in cubic kilometers. Mean and median erosion thicknesses were calculated across the valid volcanic massif analysis cells, together with the spatial distribution of estimated erosion thickness. To describe the reconstructed erosion volume relative to the modeled volcanic massif, a dimensionless denudation ratio was calculated as:

$$D = \frac{V}{\sum_{i=1}^{N}(E_i - B_i)A_i} \times 100\% \quad \ldots (12)$$

where (Bi) is the elevation of a basal reference surface fitted using elevations along the mapped geological boundary of the volcanic massif. The denominator therefore represents the modeled volume between the reconstructed reference envelope and the fitted basal surface. The resulting percentage was interpreted as a model-derived denudation ratio rather than an independently measured percentage of the original volcanic edifice removed by erosion. Because the reconstructed envelope does not necessarily represent the initial volcanic constructional surface, the calculated volume and denudation ratio describe erosion-related topographic dissection relative to the specified reference model [6, 14, 15].

2.7.1. Kriging-derived envelope scenarios

Alternative reconstructed envelopes were generated using the kriging prediction and its estimated standard deviation:

$$E_{low}(x) = max\,[\hat{Z}(x) - 1.96\ \sigma K\ (x), z(x)] \ldots (13)$$

$$E_{high}(x) = max\,[\hat{Z}(x) + 1.96\ \sigma K\ (x), z(x)] \ldots (14)$$

The corresponding reconstructed volumes were calculated using the same spatial integration procedure as the principal envelope. These scenarios were used to describe the sensitivity of the reconstructed erosion volume to kriging prediction uncertainty. Because spatial covariance among prediction errors was not explicitly propagated into an integrated-volume probability distribution, the resulting volume range was not treated as a formal 95% confidence interval for total erosional volume. Instead, it was interpreted as a conditional range associated with the selected kriging model and pointwise prediction envelopes.

2.8. Sensitivity analysis and geological-unit comparison

The sensitivity of reconstructed erosion volumes to remnant-surface selection was evaluated using three threshold scenarios: primary, strict, and relaxed. For each scenario, remnant-surface masks were generated, qualifying surfaces were aggregated into elevation control points, and a corresponding kriging envelope was reconstructed. The resulting erosion volumes and mean thicknesses were compared to determine the extent to which the estimated landscape dissection depended on the threshold criteria.

The threshold scenarios were designed to represent different degrees of selectivity rather than independent geological reconstructions of distinct paleosurfaces. The strict scenario preferentially retained more elevated, smoother terrain farther from channels. The relaxed scenario included a broader range of upper terrain surfaces, including locations with comparatively greater ruggedness and curvature. Differences among these reconstruction scenarios were therefore interpreted as sensitivity to the assumed characteristics of preserved terrain surfaces.

2.8.1. Summit-envelope comparison

An additional upper-reference scenario was constructed using a summit-envelope approach based on a maximum filter with a radius of 1 km, followed by spatial smoothing. This approach was conceptually related to topographic envelope and relief-reconstruction methods used to investigate landscape modification [4, 5].

The resulting summit envelope was compared with the present-day DEM using the same erosion-thickness and volume-integration procedures. Unlike the kriging-based reconstruction, which was constrained by morphometrically selected remnant surfaces, the summit-envelope approach represented a broader morphological reference surface derived from elevated terrain positions. Because the summit envelope was generated using a different reconstruction assumption, its volume estimate was interpreted as an alternative high-envelope scenario rather than a verified geological upper bound.

The comparison between the two approaches provided an indication of the extent to which the estimated volume depended on the conceptual definition of the reference surface.

2.8.2. Geological-unit-specific erosion characteristics

The spatial distribution of reconstructed erosion thickness was examined in relation to the mapped geological units of the Kulon Progo volcanic massif. The geological reference map [15, 17] was used to assign each valid analysis cell to one of four principal units: the Kebobutak Formation (*Tomk*), andesitic intrusions (a1), the Jonggrangan Formation (*Tmj*), or dacitic intrusions (da). For each unit, the analysis summarized its proportion of the volcanic massif, the percentage of its area identified as remnant surface, and the mean and median erosion thicknesses estimated from the primary reconstructed envelope.

These comparisons were intended to characterize the spatial association between mapped geological units and model-derived erosion thickness. Greater estimated erosion thickness within a geological unit was not assumed to demonstrate lower intrinsic resistance to weathering or erosion. Such differences may also reflect initial terrain configuration, spatial position within drainage networks, control-point coverage, structural setting, and geological map uncertainty. Accordingly, the geological-unit comparison was treated as a descriptive component of the reconstruction analysis rather than a direct test of relative rock strength.

The methodological framework therefore distinguished between three separate outputs: identification of potentially preserved terrain, spatial prediction of a reference envelope, and estimation of topographic dissection relative to that envelope. This distinction provided the basis for interpreting the reconstructed volumes and their sensitivity to methodological assumptions.

3. Results and discussion

3.1. Identification and spatial distribution of candidate remnant surfaces

The morphometric screening identified spatially discontinuous candidate remnant surfaces across the Kulon Progo paleovolcanic massif. Under the primary selection criteria, the identified surfaces occupied approximately 51.6 km², equivalent to 8.7% of the analyzed volcanic massif covering 590.8 km². Following the removal of small surface patches and spatial aggregation into 96 m blocks, these surfaces provided 10,288 elevation control points for the subsequent geostatistical reconstruction.

The spatial distribution of the selected surfaces was strongly heterogeneous (Fig. 3). Candidate remnants occurred predominantly along elevated interfluves, broad ridges, and relatively smooth upper terrain positions, whereas deeply incised valleys and strongly dissected hillslopes contained comparatively few qualifying cells. This pattern was consistent with the morphometric screening procedure, which preferentially selected relatively elevated terrain with low ruggedness, limited curvature, and greater distance from drainage channels.

The selected surfaces were characterized by a median slope of 13.9°, a median relative position of 0.68, a topographic position index (TPI) of approximately +41 m, and a median distance of 187 m from the extracted drainage network. These characteristics indicate that the identified cells generally occupied upper landscape positions rather than valley floors or strongly incised slopes.

Although the selected surfaces were relatively smooth according to the ruggedness and curvature criteria, their median slope indicates that they were not necessarily horizontal or nearly planar. Instead, they included inclined upper hillslopes and ridge surfaces whose local morphological characteristics satisfied the predefined screening thresholds. This distinction is important because the reconstruction does not require perfectly flat remnants; however, it does assume that the selected surfaces provide meaningful elevation constraints on a broader, less-dissected topographic configuration.

The distribution of candidate remnant surfaces varied substantially among the geological units. The Jonggrangan Formation exhibited the highest proportional coverage, with 14.4% of its mapped area satisfying the remnant-selection criteria. The Kebobutak Formation showed an intermediate value of 10.2%, whereas only 4.1% of the andesitic intrusion area and 1.4% of the dacitic intrusion area were classified as candidate remnants.

The spatial pattern indicates that remnant-surface occurrence was not evenly distributed among geological formations. Relatively extensive candidate remnants occurred in the Jonggrangan uplands and along northwestern ridge systems, while the southern intrusive terrain contained comparatively limited remnant coverage. These differences may reflect variations in present-day terrain dissection, local topographic position, lithological characteristics, or structural controls. However, the morphometric selection procedure cannot independently distinguish between these possible influences.

In particular, the higher proportional remnant coverage within the Jonggrangan Formation should not automatically be interpreted as evidence of greater long-term erosional resistance or better preservation of an original volcanic constructional surface. Its elevated terrain position and relatively continuous upper surfaces may also contribute to its increased likelihood of satisfying the selection criteria. Similarly, the limited remnant coverage within andesitic intrusive bodies does not independently demonstrate greater cumulative erosion or lower rock resistance. Because remnant selection depends on terrain geometry and drainage proximity, geological units occupying strongly dissected sectors may be less frequently selected irrespective of their intrinsic material properties.

The identification of 10,288 control points provided a substantial dataset for spatial interpolation. Nevertheless, the number of control points alone does not establish uniform reconstruction reliability. Because the selected observations were concentrated within morphometrically favorable terrain, some valleys and intrusive areas were constrained primarily by control points situated outside the local geological or geomorphological domain.

This spatial selectivity has direct implications for subsequent reconstruction. Areas containing extensive remnant surfaces may be relatively well represented by the interpolation dataset, whereas locations with sparse or absent control points depend more strongly on the assumed spatial covariance structure and the configuration of neighboring observations.

The identification of candidate remnant surfaces should therefore be interpreted as a reproducible terrain-screening procedure rather than independent geological confirmation of a continuous former land surface. The resulting spatial pattern provides the basis for reconstructing a reference envelope, while the validity of the geological interpretation remains dependent on assumptions about the relationship between the selected surfaces and the missing topography.

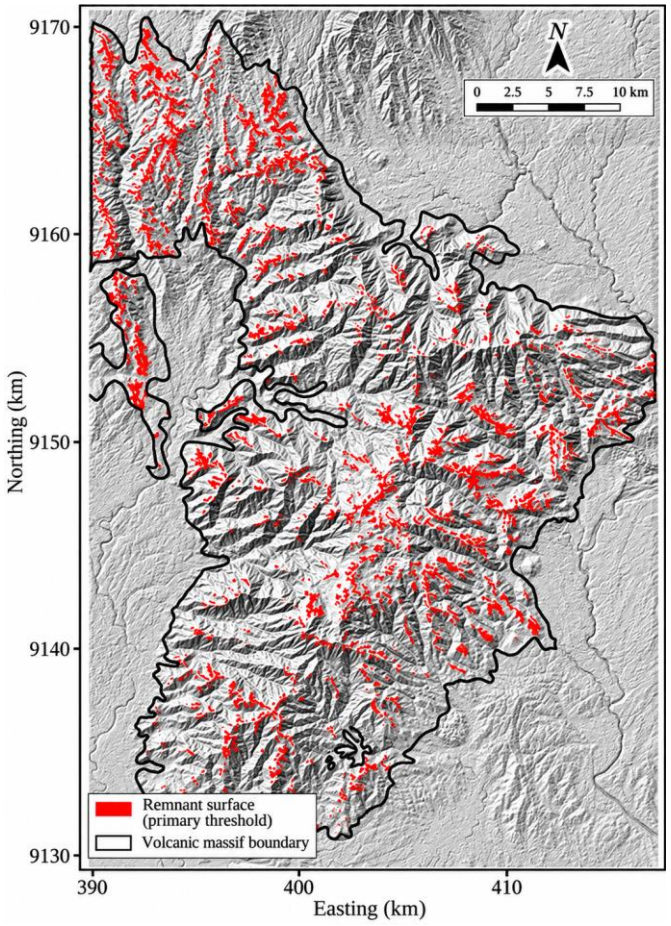


Fig. 3. Spatial distribution of candidate remnant surfaces identified using the primary morphometric threshold criteria, displayed over DEMNAS-derived shaded relief of the Kulon Progo paleovolcanic massif. The selected surfaces cover 51.6 km² (8.7% of the massif) and provide 10,288 aggregated elevation control points for the kriging-based reconstruction. The black outline indicates the volcanic massif boundary.

3.2. *Spatial dependence, semivariogram characteristics, and kriging performance*

The experimental semivariogram revealed a systematic increase in elevation semivariance with separation distance across the analyzed remnant-surface control points (Fig. 4a). Semivariance increased continuously over the investigated distance range, extending to approximately 6 km, without reaching a clearly defined sill. The observed pattern was represented using the power variogram model described in Section 2.5. The fitted parameters for the primary reconstruction were a nugget of c_0 = 55 m², a scale coefficient of b = 0.170, and a power exponent of α = 1.35.

The small nugget parameter corresponds to a square-root scale of approximately 7.4 m, suggesting that the fitted model assigned relatively limited semivariance to the shortest-distance component. However, the nugget should not be interpreted directly as an independently measured DEM vertical error because it may also incorporate unresolved short-range terrain variability and measurement effects.

The power exponent of 1.35 indicates a nonlinear increase in modeled semivariance with separation distance. This behavior is consistent with the presence of spatially organized elevation variation within the selected control-point network. Nevertheless, the absence of a sill has important implications for the interpretation of the geostatistical model. The Kulon Progo massif contains substantial regional elevation gradients associated with its dome-like morphology. Consequently, increasing semivariance may reflect a combination of spatially correlated terrain variation and a broader topographic trend.

The fitted power model therefore provides a mathematical description of the empirical semivariance over the examined range, but its agreement with the experimental values does not independently demonstrate that the elevation field satisfies all assumptions underlying ordinary kriging. The original analysis did not report separate evaluations of directional variograms, trend removal, or alternative geostatistical formulations. Accordingly, the selected model should be regarded as the adopted interpolation specification rather than a uniquely established representation of the spatial structure of the former terrain.

Despite these considerations, the spatial block cross-validation demonstrated that ordinary kriging provided relatively accurate elevation predictions at withheld remnant-surface control points (Fig. 4b). The five-fold spatial block evaluation produced a root mean square error (RMSE) of 35.6 m, a reported mean error of −5.8 m, and a coefficient of determination (R^2) of 0.95. The high R^2 indicates that the predicted elevations reproduced much of the observed variation among the withheld control-point elevations, while the RMSE quantifies the remaining prediction error in elevation units.

The reported mean error indicates a modest overall prediction bias relative to the magnitude of the terrain elevation range. However, its direction depends on the residual sign convention used in the original computation and should be interpreted consistently with the definition of mean error adopted in the Methods section. For comparison, inverse distance weighting (IDW) with a distance exponent of 2 produced an RMSE of 47.2 m. The reduction in RMSE achieved by kriging was = 24.6%. Thus, the kriging approach reduced cross-validated elevation prediction error by approximately 24.6% relative to IDW under the reported evaluation conditions. This improvement supports the usefulness of incorporating the fitted spatial dependence structure into elevation interpolation. However, it should be interpreted specifically as an improvement in withheld control-point prediction rather than as proof that the reconstructed surface accurately represents the complete former volcanic topography.

The uncertainty calibration was further examined using the kriging prediction standard deviation. Approximately 93% of the withheld elevation observations fell within the reported prediction intervals defined by the kriging estimate ±1.96 times its prediction standard deviation. This empirical coverage approached the nominal 95% level expected under an appropriately calibrated Gaussian prediction model, although the observed difference and the spatial structure of the validation data require consideration. The coverage result indicates that the kriging uncertainty estimates were broadly consistent with the prediction errors observed at the evaluated remnant points. However, it does not establish equivalent coverage in deeply incised valleys where no preserved reference elevations are available for validation. An important distinction is therefore required between interpolation performance and reconstruction

reliability. Spatial block cross validation assesses whether elevations at withheld candidate remnant points can be predicted from other control points. The principal erosion-volume calculation, in contrast, depends heavily on predicted envelope elevations above valley systems where direct observations of the former surface are unavailable.

The reported validation results support the computational performance of the selected geostatistical approach within the available control network. They do not independently confirm that all reconstructed valley-crossing surfaces represent former terrain configurations. Furthermore, the interpretation of cross-validation performance depends on how model fitting was implemented within the spatial folds. The original manuscript does not establish whether the variogram parameters were recalibrated independently for each training subset. This detail is important because model parameters estimated using observations subsequently assigned to validation folds could introduce information leakage. Overall, the geostatistical results indicate that ordinary kriging outperformed IDW for predicting withheld remnant-surface elevations and produced broadly plausible pointwise uncertainty estimates. The geological reliability of the reconstructed envelope, however, remains dependent on the spatial representativeness of the remnant observations, the variogram model, and the underlying surface-reconstruction assumptions.

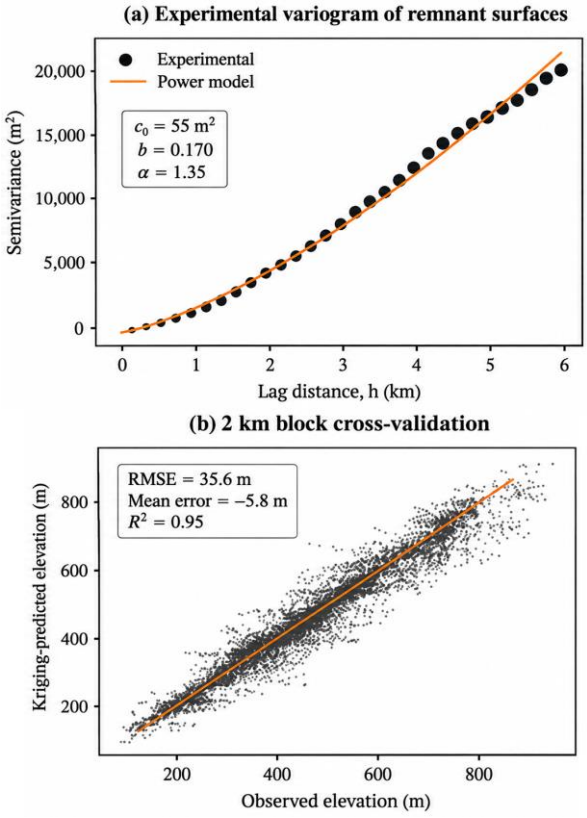


Fig. 4. Geostatistical characteristics and validation of remnant-surface elevation reconstruction: (a) experimental semivariogram and fitted power variogram model, with marker sizes proportional to the number of observation pairs, and (b) observed versus predicted control-point elevations from spatial block cross-validation using 2 × 2 km blocks. The fitted model has co = 55 m², b = 0.170, and α = 1.35. Kriging achieved an RMSE of 35.6 m and R² of 0.95.

3.3. *Reconstructed terrain envelope and spatial distribution of erosion thickness*

The ordinary kriging reconstruction produced a spatially continuous reference envelope across the analyzed Kulon Progo volcanic massif (Fig. 5a). The reconstructed elevation varied from approximately 100 m in the southern peripheral terrain to more than 900 m in the central and northern uplands. The broad spatial structure of the interpolated envelope reflected the general elevation organization of the massif, with higher reconstructed surfaces over the volcanic uplands and progressively lower elevations toward the southern margins.

The reconstructed surface was substantially smoother than the present-day DEM because its elevations were estimated from selected candidate remnant surfaces rather than from the complete topographic dataset. Consequently, the envelope bridged existing drainage depressions and represented a generalized upper terrain configuration relative to the contemporary incised topography. The difference between the reconstructed envelope and the present-day DEM was used to estimate spatially distributed erosion thickness (Fig. 5b).

The resulting erosion-thickness map exhibited pronounced spatial heterogeneity. Relatively high reconstructed thicknesses occurred primarily along major valley systems and strongly incised drainage corridors, where values commonly exceeded 100 m. In contrast, elevated ridges and broad upper terrain surfaces generally exhibited smaller differences between the reference envelope and the contemporary elevation.

This spatial organization is consistent with the interpretation that the present landscape contains substantial valley incision beneath a relatively smoother upper terrain configuration. However, the magnitude of reconstructed thickness is influenced by both observed valley depth and the interpolation assumptions used to estimate the missing reference surface.

Because the envelope was interpolated from candidate remnant elevations, the predicted surface across individual valleys was not directly constrained by measurements of the former valley-crossing topography. It therefore represents an inferred reference configuration rather than an observed historical surface. The original analysis also identified locations where the unconstrained kriging prediction was lower than the contemporary DEM. These areas accounted for approximately 17.9% of the analyzed volcanic massif. This result demonstrates that ordinary kriging did not produce an upper envelope at every location before the nonnegative erosion-thickness constraint was applied. The affected terrain occurred particularly along narrow ridges and relatively elevated surfaces that did not necessarily satisfy the complete remnant-selection criteria. Their exclusion from the control-point network may have contributed to interpolated elevations that were lower than the actual terrain.

To prevent negative modeled erosion thickness, the final envelope was defined as the maximum of the kriging prediction and the existing DEM elevation. This correction ensured that the reconstructed thickness was nonnegative throughout the analyzed region. At locations where the predicted kriging surface was below the present-day topography, the corrected erosion thickness was set to zero. Although this constraint is computationally appropriate for the adopted nonnegative thickness calculation, its application has an important interpretative consequence. Zero erosion thickness in the corrected model does not necessarily indicate an absence of historical erosion; it may simply reflect the inability of the selected interpolation model to reconstruct an envelope higher than the existing terrain.

Likewise, the correction does not independently demonstrate that the estimated upper envelope represents a physically continuous former surface. The spatial pattern of reconstructed erosion thickness therefore contains two related components: the observed geometry of contemporary terrain dissection and the modeled elevation of the reference envelope. The relative contributions of these components may differ among locations. In areas with nearby candidate remnants, the reference surface is more directly informed by selected elevation observations. In valleys or intrusive sectors containing few control points, reconstructed thickness is more strongly dependent on surrounding observations and the fitted semivariogram.

These considerations are particularly relevant when interpreting high reconstructed thicknesses within deeply incised

sectors. Although such values may indicate substantial topographic dissection, they may also be sensitive to control-point distribution, interpolation neighborhood, and assumptions about continuity across valley systems. The reconstructed thickness map should therefore be interpreted as a spatial estimate of terrain volume beneath an assumed remnant-surface envelope, rather than a direct observation of total historical rock removal [24].

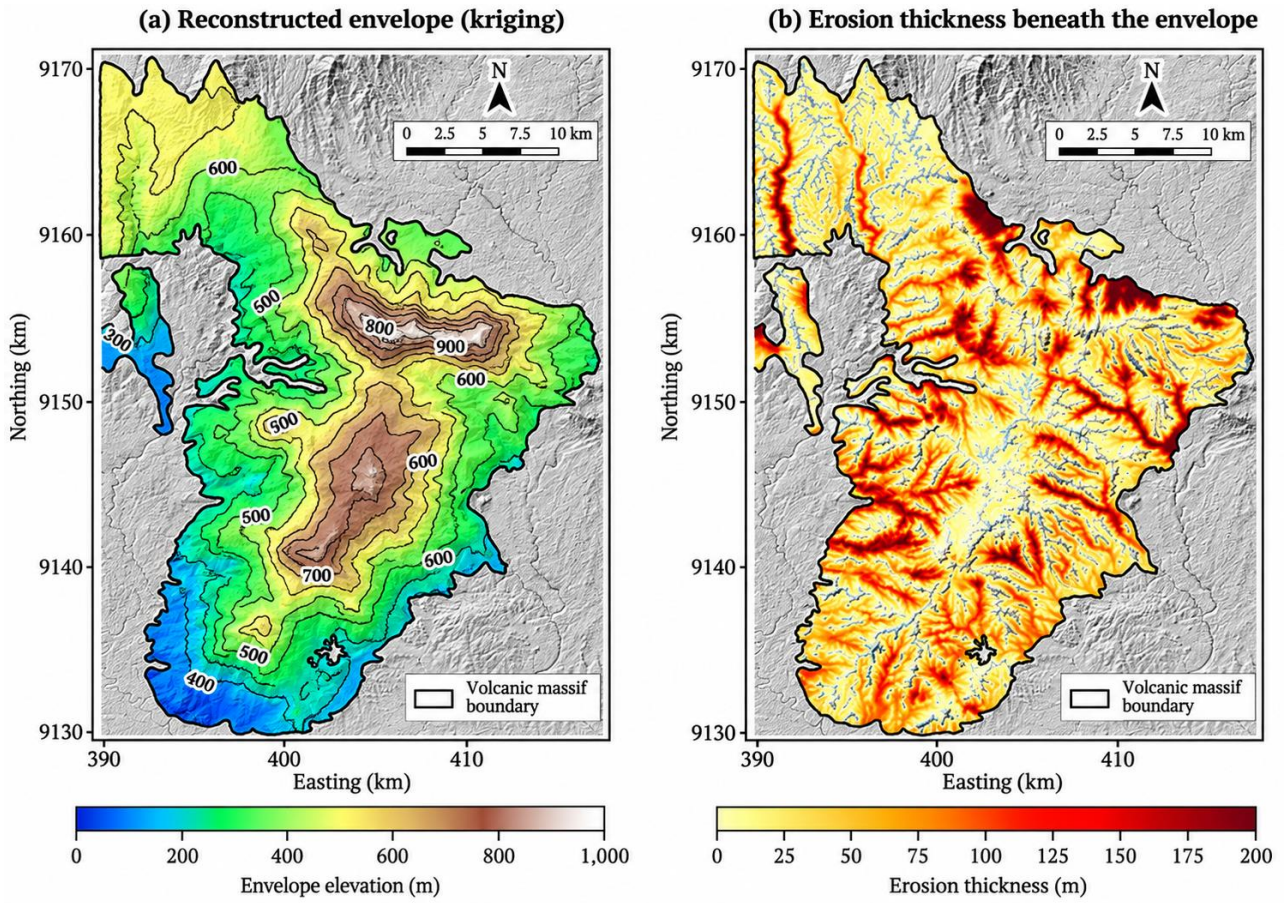


Fig. 5. Spatial reconstruction of the Kulon Progo paleovolcanic terrain: (a) ordinary kriging-derived remnant-surface envelope with 100 m elevation contours, and (b) estimated erosion thickness calculated as the nonnegative difference between the reconstructed envelope and the present-day DEMNAS elevation. High thickness values are concentrated along major incised drainage systems.

3.4. *Estimated erosion volume, denudation ratio, and reconstruction sensitivity*

The spatial integration of reconstructed erosion thickness produced an estimated eroded volume of 25.7 km³ for the primary remnant-surface reconstruction scenario (Table 2). This volume corresponded to a mean modeled erosion thickness of approximately 43 m across the volcanic massif. The distribution of erosion thickness was positively skewed, with a median value of 31 m and a 90th-percentile value of 108 m. The difference between the mean and median indicates that relatively large erosion-thickness values occurred within a smaller proportion of the landscape, particularly along deeply incised valley systems.

The mean thickness of approximately 43 m was consistent with the integrated volume and analyzed massif area. Dividing 25.7 km³ by 590.8 km² gives approximately 43.5 m, with the small difference attributable to rounding and the precise area used for numerical integration. The model-derived denudation ratio was 20.2%, calculated as the reconstructed erosion volume divided by the modeled volume between the reference envelope and the fitted basal surface. This result provides a dimensionless representation of the estimated terrain volume removed relative to the selected geometric reference model. However, the ratio should not be interpreted as an independently established percentage of the original volcanic edifice that has been removed since its construction. Its value depends on both the reconstructed envelope and the basal reference surface, which was fitted to elevations along the volcanic massif boundary.

The basal-surface construction is therefore a relevant component of the calculated denudation ratio. Because the original manuscript does not report a detailed sensitivity analysis of the basal reference, the uncertainty associated with this component remains insufficiently quantified. The principal kriging reconstruction also produced alternative erosion-volume estimates of 7.2 and 51.4 km³ using the pointwise lower and upper envelope scenarios defined by the kriging estimate ±1.96 times the prediction standard deviation. These values describe the sensitivity of integrated erosion volume to the specified prediction-envelope adjustments. They should not be interpreted as a formal 95% confidence interval for the total erosion volume because the spatial covariance of prediction errors was not explicitly propagated through the volumetric integration.

In addition, such bounds are conditional on the selected remnant-control observations, variogram specification, and spatial interpolation procedure. They do not account comprehensively for uncertainty in the geological meaning of the selected remnant surfaces or for alternative assumptions concerning former landscape geometry. A separate sensitivity analysis demonstrated that the remnant-selection criteria exerted a substantial influence on the reconstructed erosion volume. Under the strict threshold scenario, candidate remnant surfaces occupied only 16.4 km² and generated 3,595 elevation control points. This scenario yielded a kriging cross-validation RMSE of 39.0 m, compared with 47.9 m for IDW.

The corresponding estimated erosion volume increased to 43.7 km³, with a kriging-envelope scenario range of 16.0–78.4

km³. Mean erosion thickness increased to approximately 74 m, and the model-derived denudation ratio reached 30.2%. The increase in reconstructed volume was associated with the selection of fewer, more restrictive upper-terrain observations. Such observations tended to provide a higher reference envelope across portions of the incised landscape.

In contrast, the relaxed threshold scenario identified 109.0 km² of candidate remnant surfaces and generated 20,234 control points. This scenario produced a kriging RMSE of 39.2 m, compared with 45.1 m for IDW. The reconstructed erosion volume decreased to 14.4 km³, with a corresponding kriging-envelope scenario range of 2.9–33.3 km³. Mean erosion thickness decreased to approximately 24 m, and the model-derived denudation ratio was 12.4%. The reduced volume was consistent with the inclusion of a broader range of terrain surfaces, including relatively lower upper-hillslope positions that produced a lower reconstructed reference envelope.

The results demonstrate that increasing the number of control points does not necessarily improve the representativeness of the assumed pre-incision terrain configuration. Instead, the elevation and geomorphological characteristics of the selected points strongly influence the reconstructed envelope. The primary reconstruction produced the lowest kriging RMSE among the three threshold scenarios. However, differences in cross-validation RMSE alone cannot establish which threshold scenario best represents the former landscape because the validation evaluates prediction performance on different sets of selected observations.

The estimated volumes of 14.4, 25.7, and 43.7 km³ therefore represent different assumptions about the extent and geomorphological characteristics of candidate remnant surfaces. The sensitivity range of 14.4–43.7 km³ is an important result because it demonstrates that uncertainty in defining the reference surface is substantial relative to the principal volume estimate. An additional comparison was conducted using a summit-envelope reconstruction based on a smoothed maximum filter with a radius of 1 km. This approach yielded an estimated eroded volume of 100.3 km³, a mean erosion thickness of approximately 170 m, and a model-derived denudation ratio of 49.9%.

The summit-envelope volume was approximately 3.9 times the primary kriging-based estimate. This large difference highlights the sensitivity of erosion-volume calculations to the conceptual definition of the reference surface. Whereas the remnant-surface approach interpolated selected upper-terrain observations, the summit-envelope method generated a reference surface from locally high elevations, producing substantially greater modeled differences above the existing valley network. The summit-envelope reconstruction can therefore be regarded as an alternative high-envelope scenario. However, its result should not be interpreted as a proven geological upper limit because the method does not independently establish that the former landscape occupied the reconstructed elevations. Similarly, the primary kriging estimate should not be treated as a proven absolute minimum amount of material removed since volcanic construction.

The original volcanic surfaces have undergone prolonged geomorphological and geological modification, including erosion, uplift, and partial coverage by younger formations. Candidate remnant surfaces may themselves have experienced substantial lowering before the development of the present drainage network. Consequently, the estimated 25.7 km³ represents the volume between the contemporary DEM and the modeled remnant-surface envelope under the primary selection criteria. The geological interpretation of this volume is most appropriately restricted to erosion-related topographic dissection relative to the adopted reference surface.

The combined sensitivity results emphasize that reference-surface selection is a primary source of uncertainty in reconstructing eroded volcanic terrain. Although the kriging method provided relatively good interpolation performance at withheld control points, the variation among threshold scenarios and the summit-envelope reconstruction was much larger than the difference between kriging and IDW prediction errors. This distinction suggests that improving numerical interpolation accuracy alone may be insufficient to resolve the principal uncertainty in volumetric reconstruction. Establishing the geological relevance of the selected reference surface is equally important.

Table 2
Remnant-surface reconstruction and estimated erosional dissection under alternative scenarios

Reconstruction scenario	Remnant surfaces (km²)	Control points	RMSE Kriging / IDW (m)	Estimated eroded volume (km³)	Mean thickness (m)	Denudation ratio (%)
Primary thresholds	51.6	10,288	35.6 / 47.2	25.7 (7.2–51.4)	43	20.2
Strict thresholds	16.4	3,595	39.0 / 47.9	43.7 (16.0–78.4)	74	30.2
Relaxed thresholds	109.0	20,234	39.2 / 45.1	14.4 (2.9–33.3)	24	12.4
Summit envelope (1 km radius)	—	—	—	100.3	170	49.9

Note: *Values in parentheses represent volumes calculated from kriging prediction-envelope scenarios based on ±1.96σK, not formal confidence intervals for the integrated volume. The summit-envelope reconstruction provides an alternative high-envelope scenario rather than an independently validated geological upper bound. The denudation ratio is calculated relative to the modeled basal reference surface.*

3.5. Geological variation in reconstructed erosion thickness

The spatial distribution of reconstructed erosion thickness differed substantially among the mapped geological units of the Kulon Progo volcanic massif (Table 3). The Kebobutak Formation, which occupies 69.3% of the analyzed massif, exhibited a median reconstructed erosion thickness of 25 m and a mean thickness of 39 m. Approximately 10.2% of its area satisfied the primary remnant-surface identification criteria. The andesitic intrusive units, representing 25.3% of the massif, exhibited a substantially greater median reconstructed erosion thickness of 54 m and a mean thickness of 60 m.

Only 4.1% of the mapped andesite intrusion area was identified as candidate remnant surface, indicating substantially lower remnant coverage than within the Kebobutak Formation. The median reconstructed thickness within andesitic intrusive units was therefore more than twice that of the Kebobutak Formation. The Jonggrangan Formation, which occupies 4.3% of the massif, displayed the smallest reconstructed erosion thickness, with a median of 8 m and a mean of 22 m. It also exhibited the largest proportional remnant coverage (14.4%), consistent with its association with relatively continuous upper terrain surfaces.

The dacitic intrusive units occupied only 1.1% of the massif and exhibited a median reconstructed erosion thickness of 55 m and a mean of 51 m. Their remnant coverage was particularly limited, amounting to approximately 1.4% of the mapped unit area. These findings indicate that reconstructed erosion thickness varied among geological units, with relatively low values in the Jonggrangan Formation and higher values within the mapped intrusive bodies. The principal geological contrast occurred between the andesitic intrusions and the surrounding Kebobutak Formation. In the original analysis, the intrusion-related thickness contrast was also observed under the summit-envelope scenario, with median reconstructed thicknesses of approximately 206 m for andesitic intrusions and 147 m for the Kebobutak Formation.

The persistence of the contrast across two different envelope constructions suggests that the difference is not restricted to the primary kriging reference surface. However, both reconstruction approaches are influenced by the existing landscape configuration, and agreement between them does not establish the geological cause of the observed thickness differences. One

possible explanation is that some intrusive sectors experienced substantial incision associated with local drainage organization, structural discontinuities, or differences in weathering and alteration. The regional geological literature documents the complexity of the Kulon Progo volcanic system [12–15], including intrusive bodies and hydrothermally affected rock assemblages.

Fracturing and hydrothermal alteration could potentially influence rock-mass strength and susceptibility to weathering. Nevertheless, the present study did not include direct measurements of fracture density, hydrothermal alteration intensity, mechanical rock strength, or comparative weathering profiles. Accordingly, these processes remain possible explanations rather than demonstrated causes of the reconstructed erosion-thickness contrast. A second consideration is the spatial distribution of remnant-control observations. Because candidate remnants covered only 4.1% of andesitic intrusion areas, the kriging predictions within these units may have depended more strongly on control points located outside the mapped intrusion bodies. Consequently, some of the greater reconstructed thickness could reflect interpolation across strongly dissected terrain and differences in reference-surface elevation rather than the intrinsic resistance of intrusive rocks.

The geographic distribution of the intrusive units may also introduce topographic confounding. If a geological unit is preferentially exposed within valley systems or occupies particular elevations within the massif, its reconstructed erosion-thickness distribution may differ from that of another unit even in the absence of differences in intrinsic rock resistance. The regional geological map provides an additional source of uncertainty because mapped formation boundaries may include transitional or altered rock zones and may not represent the full complexity of local geological contacts.

The original results establish differences in modeled erosion thickness among geological units, but they do not isolate the independent effects of lithology, geomorphological position, structural configuration, and control-point distribution. The interpretation that andesitic intrusions are intrinsically less resistant to erosion than their surrounding volcanic rocks would therefore exceed the available evidence. A more defensible conclusion is that mapped andesitic intrusions exhibit greater reconstructed terrain dissection beneath the adopted reference envelopes than the Kebobutak Formation.

This result provides a basis for targeted geological investigation, particularly within intrusive sectors characterized by high modeled erosion thickness and limited remnant-surface coverage. Future work incorporating field observations of rock-mass strength, weathering intensity, structural discontinuities, and hydrothermal alteration would help determine whether the observed geomorphological contrast is associated with geological material properties or primarily reflects landscape position and reconstruction assumptions.

Table 3
Reconstructed erosion thickness and remnant-surface coverage by geological unit

Geological unit	Proportion of massif (%)	Remnant coverage within unit (%)	Median thickness (m)	Mean thickness (m)
Jonggrangan Formation (Tmj)	4.3	14.4	8	22
Kebobutak Formation (Tomk)	69.3	10.2	25	39
Andesitic intrusions (a1)	25.3	4.1	54	60
Dacitic intrusions (da)	1.1	1.4	55	51

Note: *Erosion thickness values correspond to the primary remnant-surface reconstruction. Remnant coverage is expressed as a percentage of the area of the corresponding geological unit. These estimates describe modeled terrain dissection and should not be interpreted as direct measurements of intrinsic lithological erosion resistance.*

3.6. Geomorphological implications and methodological limitations

The results demonstrate that DEM-based identification of candidate remnant surfaces combined with geostatistical interpolation provides a quantitative framework for examining terrain dissection in deeply modified volcanic landscapes. The reconstructed Kulon Progo envelope highlights the spatial contrast between relatively preserved upper terrain surfaces and deeply incised valley systems. The strong concentration of reconstructed erosion thickness within major drainage corridors is consistent with the importance of fluvial incision in shaping the contemporary volcanic massif. Nevertheless, the reconstruction cannot uniquely determine the former topographic configuration or the timing of terrain modification.

The Kulon Progo complex contains volcanic and intrusive units that have undergone prolonged geological evolution. The present landscape may reflect multiple episodes of volcanism, deformation, weathering, uplift, and erosion rather than a single period of regional incision. Consequently, the candidate remnant surfaces selected using contemporary terrain attributes may not all represent the same geomorphological generation or preservation age. This uncertainty is fundamental to the interpretation of reconstructed erosion volumes. The estimated volume beneath the selected envelope reflects a hypothetical upper terrain configuration conditioned on observed morphology and interpolation assumptions. It does not directly quantify all material removed since the initial formation of the volcanic edifices.

The findings also emphasize the distinction between numerical interpolation accuracy and geological reconstruction uncertainty. The reported kriging RMSE of 35.6 m demonstrates relatively favorable prediction performance at withheld remnant-control points. However, the substantial variation in erosion volumes among threshold scenarios indicates that reference-surface selection strongly influences the resulting geological estimate. For example, the primary, strict, and relaxed scenarios produced estimated volumes of 25.7, 43.7, and 14.4 km³, respectively. These differences arise from alternative definitions of qualifying remnant terrain and therefore cannot be resolved by cross-validation performance alone.

Additional uncertainty is associated with the spatial distribution of control points. Because the selection criteria exclude incised drainage positions, the reconstructed envelope is necessarily interpolated across locations with limited direct reference-surface observations. The degree of reconstruction uncertainty may therefore vary spatially according to control-point density, distance to neighboring observations, geomorphological complexity, and the adopted semivariogram.

The original analysis assessed prediction uncertainty using kriging standard deviations and evaluated interpolation performance through spatial block cross-validation. However, it did not provide a spatial comparison of erosion thickness, prediction uncertainty, and control-point distance. Such a comparison would be particularly valuable for determining whether areas of high reconstructed erosion thickness are also associated with weaker observational constraints. The assumption of spatial dependence represented by the power variogram also requires further evaluation. The continuously increasing semivariance observed in the Kulon Progo control-point elevations may reflect a combination of spatial covariance and the broad regional elevation trend. Because directional anisotropy and alternative trend-based kriging formulations were not examined, the potential effect of these factors on the reconstructed envelope remains unresolved.

The spatial resolution of the interpolation constitutes another methodological consideration. The original kriging surface was predicted on a 100 m grid and subsequently resampled to 16 m for comparison with the contemporary DEM. This procedure produced a common spatial grid for erosion-thickness calculations, but interpolation to a finer raster spacing did not restore terrain detail absent from the initial 100 m prediction. Sensitivity testing using alternative kriging prediction resolutions would help determine whether the estimated total volume and spatial pattern of erosion thickness depend substantially on the

DEM representation and terrain-attribute extraction introduce additional uncertainty. DEMNAS may partly represent vegetation or aboveground features in densely vegetated regions [16]. Such effects could influence ruggedness, curvature, and the selection of candidate remnant surfaces. Furthermore, the drainage network was extracted using a fixed contributing-area threshold. Variations in channel initiation conditions, terrain resolution, and depression filling may affect channel-distance calculations and consequently the spatial extent of identified remnant surfaces.

The exclusion of a narrow western sector of the volcanic dome because of the available DEM tile coverage also limits the geographic completeness of the reconstructed massif. The comparison among geological units must likewise be interpreted in the context of spatial heterogeneity. The higher reconstructed erosion thickness within andesitic intrusions may be influenced by terrain position, drainage organization, geological map boundaries, and the limited distribution of remnant-control points.

The available results do not demonstrate that the mapped intrusive bodies have lower intrinsic rock strength or greater susceptibility to long-term erosion. The lack of independent geological validation represents an important limitation. Field observations of potentially preserved surfaces, structural relationships, weathering characteristics, and rock-mass strength would provide additional evidence regarding the geological significance of the reconstructed envelope.

Similarly, independent geophysical measurements could contribute constraints on subsurface geological structure where sufficient contrasts in physical properties exist. Gravity observations, for example, may help investigate the geometry of subsurface intrusive bodies if density contrasts between the intrusions and surrounding rocks are adequate. However, geophysical integration would not independently establish the former land-surface elevation without additional geological and geomorphological constraints.

A further limitation concerns the absence of chronological information. Although the reconstruction provides a volumetric estimate of terrain dissection, the analysis does not establish when incision began or how the magnitude of erosion varied through time. Accordingly, the estimated volume cannot be converted into an erosion rate without independent constraints on the duration of the relevant geomorphological processes.

Future investigations should prioritize field verification of candidate remnant surfaces, assessment of the regional elevation trend and variogram anisotropy, sensitivity analysis of control-point aggregation and kriging neighborhood size, and evaluation of the influence of prediction-grid resolution on integrated erosion volume. Additional analysis of control-point distance and spatial prediction uncertainty would also help identify areas where reconstructed erosion thickness is strongly or weakly constrained by the available observations.

Despite these limitations, the study provides useful quantitative information on terrain dissection within the Kulon Progo paleovolcanic massif. The reconstructed erosion-volume scenarios demonstrate the substantial influence of reference-surface assumptions, while the geological-unit comparisons identify spatial contrasts that may guide subsequent geomorphological and geological investigation. The broader methodological implication is that DEM-based envelope reconstruction should be evaluated not only through interpolation accuracy but also through the geological plausibility of the reference surface, spatial representativeness of control observations, and sensitivity of integrated volume estimates. By explicitly separating these components, the present framework provides a more transparent basis for investigating erosion-related topographic modification in deeply dissected paleovolcanic landscapes.

4. Conclusion

This study quantified model-derived erosional dissection in the Kulon Progo paleovolcanic complex, Indonesia, by integrating DEMNAS-based morphometric screening, remnant-surface identification, and ordinary kriging reconstruction. The primary selection criteria identified 51.6 km² of candidate remnant surfaces, representing 8.7% of the 590.8 km² volcanic massif, and generated 10,288 elevation control points. Ordinary kriging with a power variogram achieved a spatial block cross-validation RMSE of 35.6 m and R^2 of 0.95, corresponding to a 24.6% reduction in RMSE relative to inverse distance weighting (47.2 m). The reconstructed reference envelope yielded an estimated erosion volume of 25.7 km³, a mean erosion thickness of approximately 43 m, and a model-derived denudation ratio of 20.2%. However, the estimated volume was sensitive to the definition of candidate remnant surfaces, ranging from 14.4 to 43.7 km³ under relaxed and strict threshold scenarios, respectively. An alternative summit-envelope reconstruction produced a substantially larger estimate of 100.3 km³, emphasizing the strong dependence of reconstructed erosion volumes on the assumed reference surface.

The spatial reconstruction revealed that modeled erosion thickness was concentrated along major incised drainage systems, while relatively low values characterized elevated interfluves and upper terrain surfaces. Geological-unit comparisons indicated greater median reconstructed erosion thickness within andesitic intrusions (54 m) than within the Kebobutak Formation (25 m), although this difference cannot be attributed directly to contrasting rock resistance without additional geological and mechanical evidence. The results demonstrate that DEM-based kriging reconstruction can provide a reproducible framework for quantifying erosion-related terrain dissection, but interpolation accuracy at remnant-surface control points does not independently establish the geological validity of the reconstructed former terrain. The resulting volume estimates are therefore conditional on remnant-surface selection, spatial interpolation assumptions, and the adopted geological framework. Future investigations should incorporate independent field verification, sensitivity testing of interpolation parameters, and geological or geophysical observations to better constrain the reconstructed reference surface and assess the factors controlling erosional modification within the Kulon Progo paleovolcanic complex.

CRediT authorship contribution statement

Rizqi Prastowo: Writing – review & editing, Writing – original draft, Supervision, Software, Resources, Methodology, Investigation, Formal analysis, Data curation. **Ignatius Adi Prabowo:** Writing – review & editing, Writing – original draft, Investigation, Formal analysis.

Declaration of Competing Interest

The authors declare that they have no known competing financial interests or personal relationships that could have appeared to influence the work reported in this paper.

Data availability

Data will be made available on request.

Acknowledgment

The author gratefully acknowledges the Geospatial Information Agency of Indonesia (Badan Informasi Geospasial, BIG) for providing access to the Indonesian National Digital Elevation Model (DEMNAS), which served as the primary topographic dataset for this study. Appreciation is also extended to the Geological Agency of Indonesia (Badan Geologi), particularly the Geological Research and Development Centre, for providing the geological map data used to delineate the Kulon Progo volcanic massif and characterize its geological units.

References

1. Grosse, P., van Wyk de Vries, B., Euillades, P. A., Kervyn, M., and Petrinovic, I. A. (2012). Systematic Morphometric Characterization of Volcanic Edifices Using Digital Elevation Models, Geomorphology, Vol. 136, No. 1, pp. 114–131. doi:10.1016/j.geomorph.2011.06.001.
2. Karátson, D., Telbisz, T., and Wörner, G. (2012). Erosion Rates and Erosion Patterns of Neogene to Quaternary Stratovolcanoes in the Western Cordillera of the Central Andes: An SRTM DEM Based Analysis, Geomorphology, Vols. 139–140, pp. 122–135. doi:10.1016/j.geomorph.2011.10.010.
3. Lahitte, P., Samper, A., and Quidelleur, X. (2012). DEM-Based Reconstruction of Southern Basse-Terre Volcanoes (Guadeloupe Archipelago, FWI): Contribution to the Lesser Antilles Arc Construction Rates and Magma Production, Geomorphology, Vol. 136, No. 1, pp. 148–164. doi:10.1016/j.geomorph.2011.04.008.
4. Small, E. E., and Anderson, R. S. (1998). Pleistocene Relief Production in Laramide Mountain Ranges, Western United States, Geology, Vol. 26, No. 2, pp. 123–126. doi:10.1130/0091-7613(1998)026<0123>2.3.CO;2.
5. Brocklehurst, S. H., and Whipple, K. X. (2002). Glacial Erosion and Relief Production in the Eastern Sierra Nevada, California, Geomorphology, Vol. 42, No. 1–2, pp. 1–24. doi:10.1016/S0169-555X(01)00069-1.
6. De Reu, J., Bourgeois, J., Bats, M., Zwertvaegher, A., Gelorini, V., De Smedt, P., Chu, W., Antrop, M., De Maeyer, P., Finke, P., Van Meirvenne, M., Verniers, J., and Crombé, P. (2013). Application of the Topographic Position Index to Heterogeneous Landscapes, Geomorphology, Vol. 186, pp. 39–49. doi:10.1016/j.geomorph.2012.12.015.
7. Sappington, J. M., Longshore, K. M., and Thompson, D. B. (2007). Quantifying Landscape Ruggedness for Animal Habitat Analysis: A Case Study Using Bighorn Sheep in the Mojave Desert, Journal of Wildlife Management, Vol. 71, No. 5, pp. 1419–1426. doi:10.2193/2005-723.
8. Matheron, G. (1963). Principles of Geostatistics, Economic Geology, Vol. 58, No. 8, pp. 1246–1266. doi:10.2113/gsecongeo.58.8.1246.
9. Oliver, M. A., and Webster, R. (1990). Kriging: A Method of Interpolation for Geographical Information Systems, International Journal of Geographical Information Systems, Vol. 4, No. 3, pp. 313–332. doi:10.1080/02693799008941549.
10. Cressie, N. (1985). Fitting Variogram Models by Weighted Least Squares, Journal of the International Association for Mathematical Geology, Vol. 17, No. 5, pp. 563–586. doi:10.1007/BF01032109.
11. Roberts, D. R., Bahn, V., Ciuti, S., Boyce, M. S., Elith, J., Guillera-Arroita, G., Hauenstein, S., Lahoz-Monfort, J. J., Schröder, B., Thuiller, W., Warton, D. I., Wintle, B. A., Hartig, F., and Dormann, C. F. (2017). Cross-Validation Strategies for Data with Temporal, Spatial, Hierarchical, or Phylogenetic Structure, Ecography, Vol. 40, No. 8, pp. 913–929. doi:10.1111/ecog.02881.
12. van Bemmelen, R. W. (1949). The Geology of Indonesia, Vol. IA, Government Printing Office and Martinus Nijhoff, The Hague, Netherlands.
13. Syafri, I., Budiadi, E., and Sudradjat, A. (2013). Geotectonic Configuration of Kulon Progo Area, Yogyakarta, Indonesian Journal on Geoscience, Vol. 8, No. 4, pp. 185–190. doi:10.17014/ijog.8.4.185-190.
14. Hartono, H. G., and Sugarbo, O. (2026). Volcano Stratigraphy of Kulon Progo Super Brigade, Indonesian Journal on Geoscience, Vol. 13, No. 1, pp. 143–157. doi:10.17014/ijog.13.1.143-157.
15. Rahardjo, W., Sukandarrumidi, and Rosidi, H. M. D. (1995). Peta Geologi Lembar Yogyakarta, Jawa, Scale 1:100,000, Pusat Penelitian dan Pengembangan Geologi, Bandung, Indonesia.
16. Julzarika, A., and Harintaka. (2019). Indonesian DEMNAS: DSM or DTM?, Proceedings of the IEEE Asia-Pacific Conference on Geoscience, Electronics and Remote Sensing Technology (AGERS), Jakarta, Indonesia, pp. 31–36. doi:10.1109/AGERS48446.2019.9034351.
17. Pusat Penelitian dan Pengembangan Geologi. (2010). Peta Geologi Indonesia, Digital GIS Dataset (Geologi.shp), Badan Geologi, Bandung, Indonesia.
18. Ihsan, H. M., and Sahid. (2021). Vertical Accuracy Assessment on Sentinel-1, ALOS PALSAR, and DEMNAS in the Ciater Basin, Jurnal Geografi Gea, Vol. 21, No. 1, pp. 16–25.
19. O'Callaghan, J. F., and Mark, D. M. (1984). The Extraction of Drainage Networks from Digital Elevation Data, Computer Vision, Graphics, and Image Processing, Vol. 28, No. 3, pp. 323–344. doi:10.1016/S0734-189X(84)80011-0.
20. Zevenbergen, L. W., and Thorne, C. R. (1987). Quantitative Analysis of Land Surface Topography, Earth Surface Processes and Landforms, Vol. 12, No. 1, pp. 47–56. doi:10.1002/esp.3290120107.
21. Horn, B. K. P. (1981). Hill Shading and the Reflectance Map, Proceedings of the IEEE, Vol. 69, No. 1, pp. 14–47. doi:10.1109/PROC.1981.11918.
22. Shepard, D. (1968). A Two-Dimensional Interpolation Function for Irregularly-Spaced Data, Proceedings of the 23rd ACM National Conference, pp. 517–524. doi:10.1145/800186.810616. Abrahamson, N. A., Gregor, N., and Addo, K. (2016). BC Hydro Ground Motion Prediction Equations for Subduction Earthquakes, *Earthquake Spectra*, Vol. 32, No. 1, 23–44. doi:10.1193/051712EQS188MR.